Draft version April 9, 2015
Preprint typeset using LaTeX style emulateapj v. 5/2/11

DISCOVERY OF EIGHT $Z \sim 6$ QUASARS IN THE SLOAN DIGITAL SKY SURVEY OVERLAP REGIONS

Linhua Jiang[1,2], Ian D. McGreer[3], Xiaohui Fan[3], Fuyan Bian[4,6], Zheng Cai[3], Benjamin Clément[3], Ran Wang[1], and Zhou Fan[5]

Draft version April 9, 2015

ABSTRACT

We present the discovery of eight quasars at $z \sim 6$ identified in the Sloan Digital Sky Survey (SDSS) overlap regions. Individual SDSS imaging runs have some overlap with each other, leading to repeat observations over an area spanning >4000 deg^2 (more than 1/4 of the total footprint). These overlap regions provide a unique dataset that allows us to select high-redshift quasars more than 0.5 mag fainter in the z band than those found with the SDSS single-epoch data. Our quasar candidates were first selected as i-band dropout objects in the SDSS imaging database. We then carried out a series of follow-up observations in the optical and near-IR to improve photometry, remove contaminants, and identify quasars. The eight quasars reported here were discovered in a pilot study utilizing the overlap regions at high galactic latitude ($|b| > 30$ deg). These quasars span a redshift range of $5.86 < z < 6.06$ and a flux range of $19.3 < z_{\rm AB} < 20.6$ mag. Five of them are fainter than $z_{\rm AB} = 20$ mag, the typical magnitude limit of $z \sim 6$ quasars used for the SDSS single-epoch images. In addition, we recover eight previously known quasars at $z \sim 6$ that are located in the overlap regions. These results validate our procedure for selecting quasar candidates from the overlap regions and confirming them with follow-up observations, and provide guidance to a future systematic survey over all SDSS imaging regions with repeat observations.

Subject headings: cosmology: observations — quasars: general — quasars: emission lines

1. INTRODUCTION

High-redshift quasars provide a powerful tool to study the early universe. The first $z \sim 6$ quasars (e.g. Fan et al. 2001, 2003, 2004) were found by the Sloan Digital Sky Survey (SDSS; York et al. 2000). Most of these quasars are very luminous ($M_{1450} < -26$ mag). Deep near-IR spectroscopy has shown that these quasars harbor billion-solar-mass black holes and emit near the Eddington limit, suggesting the rapid growth of central black holes in the early epoch (e.g. Jiang et al. 2007; Kurk et al. 2007). Their broad emission lines exhibit solar or supersolar metallicity, indicating that vigorous star formation and element enrichment have occurred in the host galaxies (e.g. Jiang et al. 2007; Kurk et al. 2007; De Rosa et al. 2011). Their optical absorption spectra show that the state of the intergalactic medium (IGM) at $z \sim 6$ is close to the reionization epoch (e.g. Fan et al. 2006b; Carilli et al. 2010; McGreer et al. 2011). Furthermore, the mid/far-infrared, mm/sub-mm, and radio observations of these quasars have provided rich information about dust emission and star formation in their host galaxies (e.g. Walter et al. 2009; Jiang et al. 2010; Wang et al. 2011, 2013). Therefore, $z \geq 6$ quasars are essential to understanding black hole accretion, galaxy evolution, and the IGM state in the first billion years of cosmic time.

In recent years, more than 70 quasars at $z \sim 6$ have been discovered. The SDSS pioneered quasar studies at these redshifts, followed by the Canada-France High-redshift Quasar Survey (CFHQS; Willott et al. 2005) and the UKIRT Infrared Deep Sky Survey (UKIDSS; Warren et al. 2007). To date ∼30 quasars have been discovered in the main imaging survey (e.g. Fan et al. 2001, 2003, 2004, 2006a) and the Stripe 82 deep survey (Jiang et al. 2008, 2009). The UKIDSS has found several quasars (Venemans et al. 2007; Mortlock et al. 2009, 2011), including the most distant quasar known at $z = 7.08$ (Mortlock et al. 2011). The CFHQS produced 20 quasars down to a fainter luminosity limit (Willott et al. 2007, 2009, 2010). Most recently, two large surveys, the Panoramic Survey Telescope & Rapid Response System 1 (Pan-STARRS1) and the Visible and Infrared Survey Telescope for Astronomy (VISTA) Kilo-Degree Infrared Galaxy (VIKING) survey have started to yield high-redshift quasars. Pan-STARRS1 is sensitive mainly to brighter quasars than SDSS but over a much larger area, and $\gtrsim$10 new quasars at $z \sim 6$ have been published from this survey (Morganson et al. 2012; Bañados et al. 2014), including three quasars at $6.5 < z < 6.7$ (Venemans et al. 2015). VIKING data have also been used to discover three quasars at $z > 6.5$ (Venemans et al. 2013). The number of high-redshift known quasars is increasing steadily.

In this paper we introduce a new method for finding $z \sim 6$ quasars by using regions with overlapping imaging in the SDSS. The SDSS imaging survey was conducted in drift scan mode along great circles, and the imaging runs usually overlap with each other due to the survey geometry and strategy. This results in multiple observations

[1] Kavli Institute for Astronomy and Astrophysics, Peking University, Beijing 100871, China; jiangKIAA@pku.edu.cn
[2] School of Earth and Space Exploration, Arizona State University, Tempe, AZ 85287-1504, USA
[3] Steward Observatory, University of Arizona, 933 North Cherry Avenue, Tucson, AZ 85721, USA
[4] Research School of Astronomy and Astrophysics, Australian National University, Weston Creek, ACT 2611, Australia
[5] Key Laboratory of Optical Astronomy, National Astronomical Observatories, Chinese Academy of Sciences, Beijing 100012, China
[6] Stromlo Fellow

of individual sources within the overlap regions. About one-quarter of the sky area covered by the SDSS has multiple imaging coverage. These overlap regions allow us to select quasars that are fainter than those found in the SDSS single-epoch images. They ensure that quasar candidates are free of spurious detections (such as cosmic rays), which is particularly useful for objects with single-band (z-band in this paper) detections. Here we report eight new quasars found in our first search of $z \sim 6$ quasars in the overlap regions. These quasars are $\sim$0.5 mag fainter than the quasars selected from SDSS single-epoch data.

The layout of the paper is as follows. In Section 2 we briefly describe the SDSS overlap regions. In Section 3 we introduce our quasar selection procedure and follow-up observations. We present the new quasars in Section 4, and summarize the paper in Section 5. Throughout the paper SDSS magnitudes are reported on the AB system instead of the asinh system (Lupton et al. 1999), and all near-IR magnitudes are on the Vega system. We use a Λ-dominated flat cosmology with $H_0 = 70$ km s^{-1} Mpc^{-1}, $\Omega_m = 0.3$, and $\Omega_\Lambda = 0.7$.

2. SDSS OVERLAP REGIONS

In this section we describe the SDSS overlap regions, the regions that were scanned by two or more SDSS imaging runs. The SDSS imaging survey was carried out in drift-scan mode using a 142 mega-pixel camera (Gunn et al. 1998, 2006). An SDSS run (strip) consists of 6 parallel scanlines (camera columns) for each of five *ugriz* bands (Fukugita et al. 1996). The scanlines are 13.′5 wide with gaps of roughly the same width, so two interleaving strips make a stripe. SDSS scanlines are divided into fields, and a field is the union of five *ugriz* frames covering the same region of sky. Processing of individual runs includes assessments of the photometric quality (Ivezić et al. 2004; Hogg et al. 2001).

The SDSS imaging runs generally overlap each other, due to the survey geometry and strategy (Stoughton et al. 2002). The imaging survey in drift-scan mode was along great circles, and had two common poles at [R.A., Decl.] = [95°, 0°] and [270°, 0°]. The fields overlap more substantially when they approach the survey poles (Figure 1). In addition, the two interleaving strips that make any stripe slightly overlap, leading to duplicate observations in a small area. Furthermore, if the quality of a run, or part of a run, did not meet the SDSS standard criteria, the relevant region of this run was re-observed, yielding duplicate observations in this region. Obviously, a combination of the above reasons may result in more than two observations in some regions.

The upper panel in Figure 1 shows the coverage of the SDSS overlap regions at high galactic latitude $|b| > 30°$. The SDSS deep stripe, Stripe 82, has been excluded, because it has much deeper co-added data (Jiang et al. 2014; Annis et al. 2014). The data points represent bright ($19.0 < r < 19.1$) point sources with at least two observations. In the lower panel of the figure, the coverage map is zoomed in to an area of R.A. = 180°–220° and Decl. = 20°–40°, where the data points are point sources with $19 < r < 20$. We estimated the total area of the overlap regions in the upper panel by calculating the area occupied by the actual data points. The sources

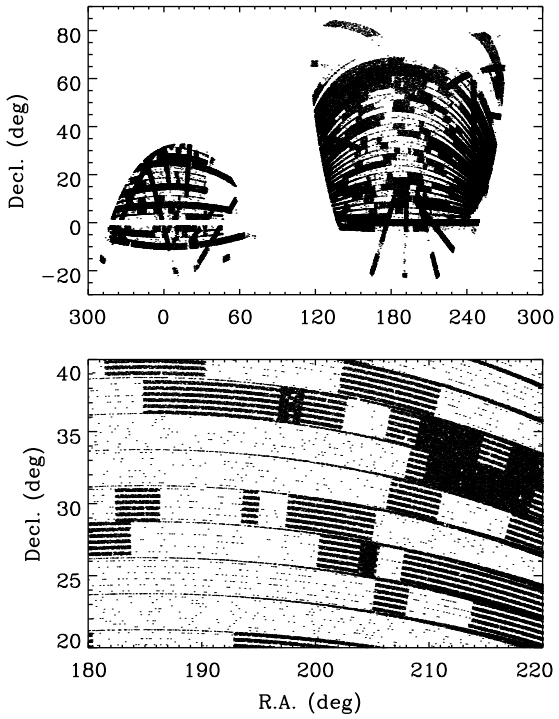

Figure 1. Upper panel: coverage of the SDSS overlap regions at high galactic latitude $|b| > 30$. Stripe 82 has been excluded. The data points represent bright ($19.0 < r < 19.1$) point sources with at least two SDSS observations. Lower panel: a closer look at an area of R.A. = 180°–220° and Decl. = 20°–40°. The data points represent point sources with $19 < r < 20$. We can clearly see individual scanlines.

we used are point sources with $19 < r < 21$. We divided the R.A.–Decl. plane into small grid elements, where each element measures 0.05° at a side. If a grid element contains more than one object, it was assumed to be covered by the overlap regions. The total area by summing the area of all selected grid elements is 3700 square degrees. This rough estimate is accurate to roughly 10%, and could be improved by using more sources and by refining grid elements. We leave this for a future work. The total area of all SDSS overlap regions, including low galactic latitude $|b| < 30°$, is more than 4000 square degrees.

For a given source in the overlap regions, the SDSS pipeline selects one detection as a 'primary' detection from a 'primary' run/field. Additional detections are classified as 'secondary'. The primary runs/fields are generally deeper due to better image quality in terms of seeing, sky background, atmospheric transparency, etc. Figure 2 illustrates the difference between primary and secondary detections in the z band. The sources used in the figure are point sources with $z < 21$ mag, selected from the overlap regions displayed in the lower panel of Figure 1 (R.A. = 180°–220° and Decl. = 20°–40°). The upper panel of Figure 2 shows photometric errors versus z-band magnitude. The shaded regions include central 68% of the sources at any magnitude. They indicate that primary detections have slightly better data quality than secondary detections. This is also suggested by the three lower panels, which show the distribution of photometric errors in three different magnitude bins. Compared to primary detections, the distribution of errors for the secondary detections has a longer tail towards greater errors.

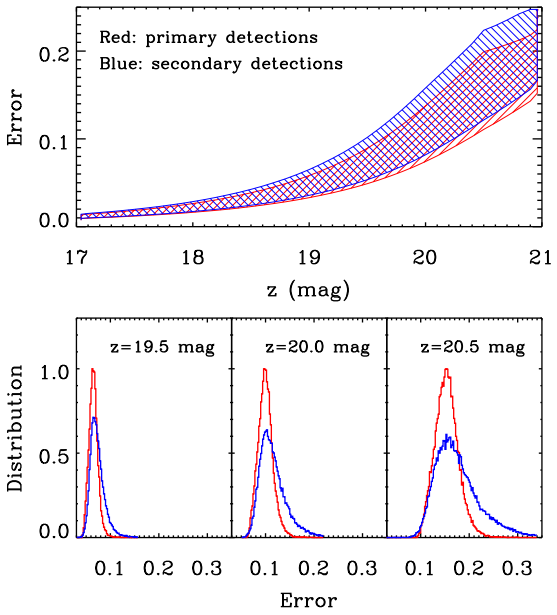

Figure 2. Comparison between primary and secondary detections in the z band. The sources used in the figure are point sources with $z < 21$ mag, selected from the overlap regions displayed in the lower panel of Figure 1 (R.A. = 180°–220° and Decl. = 20°–40°). The upper panel shows photometric errors versus z-band photometry. The shaded regions include central 68% sources at any magnitude. They indicate that primary detections have slightly better data quality than secondary detections. The three lower panels show the distribution of photometric errors at three different magnitudes. Compared to primary detections, secondary detections have longer distribution tails towards larger errors.

Therefore, a secondary detection does not always significantly improve the photometry of a source. However, it generally rules out the possibility that its primary detection is a false detection. This is particularly important for single-band detected sources, such as $z \geq 6$ quasars.

3. QUASAR CANDIDATE SELECTION AND FOLLOW-UP OBSERVATIONS

In this section we present the details of our candidate selection and spectroscopic identification of $z \sim 6$ quasars in the SDSS overlap regions. The selection procedure is similar to the procedures that were used to select SDSS $z \sim 6$ quasars in previous studies (e.g. Fan et al. 2001, 2003; Jiang et al. 2008, 2009). The procedure consists of several steps as shown in the following subsections.

3.1. *Selection of i-band Dropout Objects*

We start with SDSS Data Release 9 (DR9) 'primary' sources at high galactic latitude $|b| > 30°$, by using the 'photoPrimary' table with the SDSS Query/CasJobs online server, excluding Stripe 82. The 'photoPrimary' table includes both point and extended sources. Although distant quasars are point-like objects in ground-based images, faint point-like objects could be mis-classified as extended objects (and vice versa); thus we include extended objects. We then remove sources with critical SDSS processing flags such as BRIGHT, EDGE and SATUR. For each source, we searched for 'neighbors' ('secondary' detections from different runs) within a $0\farcs5$ radius. All matched pairs are considered to be multiple observations of the same object. From these dual observations we select i-band dropout objects using the following color cuts,

$$g > 24.0, \quad (1)$$
$$r - z > 3.0, \quad (2)$$
$$i - z > 2.2, \quad (3)$$
$$\text{and } \sigma_z < 0.155. \quad (4)$$

These selection criteria are applied to the individual observations, i.e., each of the dual observations must meet the criteria except criterion 4. We require that the primary detections meet criterion 4 (at least 7σ detections), and the secondary detections should be detected at a significance of $> 5\sigma$. In this first step, we obtain a total of $\sim$550 i-band dropout objects.

In the previous search of luminous $z \sim 6$ quasars with the SDSS single-epoch images (see Fan et al. papers), the magnitude limit was roughly $z = 20$ (10σ detections). Below 10σ, the number of contaminants in i-dropout selection increases dramatically. From single-epoch images, one would get tens of thousands of i-dropout candidates down to a 7σ threshold, where the vast majority of them are spurious objects. Using duplicate observations ensures that most of the i-dropout objects we select are physical sources.

We visually inspect the dropouts in the SDSS *ugriz* images, and remove obvious contaminants, such as suspicious detections close to very bright stars and objects that are apparently extended. We reject about one-third of the 550 objects in this step. We then remove previously known objects, such as L/T dwarfs and $z \sim 6$ quasars. We match our objects to the list of known L/T dwarfs from `DwarfArchives.org`, and find 51 known dwarfs. We also match the objects to the list of i-dropouts that have been spectroscopically identified as non-quasars during our previous searches for $z \sim 6$ quasars. In addition, we find that 8 objects are previously discovered quasars at $z \sim 6$. These quasars are summarized in Table 1. They are generally brighter than $z = 20$ mag. After removing these objects, about 250 objects remain in our candidate list.

We match the remaining objects to the 2MASS catalog (Skrutskie et al. 2006) and to the catalog of the UKIRT Infrared Deep Sky Survey (UKIDSS; Lawrence et al. 2007). We obtain 10 matches from the 2MASS, and 53 matches from the UKIDSS, providing near-IR photometry for 63 objects. The majority are then rejected as quasar candidates based on their location in the $z - J$ versus $i - z$ color-color diagram (see section 3.3). This leaves a total of 190 i-dropout candidates selected for additional observations.

3.2. *Improving the i and z-band Photometry*

The next step is to improve the i and z-band photometry. The majority of the objects have z-band detections weaker than 10σ. For these objects we obtained deeper i and z band images using the wide-field optical imager 90Prime on the 2.3m Bok telescope. The typical integration time was 5 min per object (single exposure) in the i band and 3 min per object (single exposure) in the z band. The observing conditions for many objects were poor-to-moderate with significant moonlight, poor seeing, or non-photometric transparency, because most of them were observed as backup targets for other programs. To date we have observed roughly 110 objects.

Table 1
Previously Known Quasars in the SDSS Overlap Regions

Quasar (SDSS)	Redshift	i (mag)	z (mag)	Reference
J000239.40+255034.8	5.80	21.49±0.12	18.94±0.05	Fan et al. (2004)
		21.39±0.13	18.88±0.05	
J084119.52+290504.4	5.96	23.30±0.66	19.78±0.13	Goto (2006)
		22.47±0.28	19.78±0.09	
J103027.09+052455.0	6.28	22.93±0.41	19.59±0.08	Fan et al. (2001)
		23.14±0.42	19.91±0.11	
J104433.04–012502.1	5.80	21.58±0.20	18.99±0.07	Fan et al. (2000)
		21.62±0.16	19.09±0.07	
J131911.29+095051.3	6.13	21.79±0.33	19.35±0.14	Mortlock et al. (2009)
		22.69±0.28	20.07±0.10	
J141111.28+121737.3	5.93	22.91±0.35	19.55±0.08	Fan et al. (2004)
		23.49±0.42	19.56±0.07	
J162331.81+311200.6	6.22	> 24	19.64±0.10	Fan et al. (2004)
		24.47±0.85	20.06±0.15	
J163033.90+401209.7	6.05	23.42±0.39	20.33±0.12	Fan et al. (2003)
		22.69±0.27	20.14±0.11	

Note. — The multiple entries for the i and z band photometry are from SDSS duplicate observations.

The 90Prime images were reduced in a standard fashion using our own `IDL` routines. First we made master bias and flat images from bias and flat images taken in the same night. A bad pixel mask was created from the flat image. Then science images were overscan and bias corrected and flat-fielded. Saturated pixels and bleeding trails were identified, and incorporated (along with the bad mask) into weight images. Next the first-round sky subtraction was performed by fitting a low-order 2D polynomial function to the background. The 90Prime CCDs are thin chips, so they produce strong fringing in the i and z bands. We removed fringes in two iterations. Then another round of sky subtraction was performed. We detected objects using `SExtractor` (Bertin & Arnouts 1996) and calculated astrometric solutions using `SCAMP` (Bertin 2006) by matching objects to the SDSS. Photometry was measured within an aperture (diameter) size of 8 pixels ($\sim 3\farcs6$) and calibrated by matching a large number of nearby bright point sources to the SDSS.

With the improved i and z band photometry, we rejected objects with relatively blue $i-z$ colors. The 90Prime i and z filters are slightly redder than the SDSS i and z filters. Depending the strength of Lyα emission, quasars at $5.7 < z < 6.0$ could have much bluer $i-z$ colors in the 90Prime system. We rejected objects with $i-z < 1.8$ (in the 90Prime system), instead of $i-z < 2.2$ (in the SDSS filter system) that was used in our previous studies. This is similar to the color cut used by the CFHQS (e.g., Willott et al. 2007).

3.3. *Near-IR Photometry and Optical Spectroscopy*

The next step is to obtain near-IR (J and/or Y band) photometry. We excluded objects that already have J-band photometry from the 2MASS or the UKIDSS (section 3.1). Near-IR observations for the other objects were obtained with the MMT SWIRC (Brown et al. 2008) and the KPNO 4m NEWFIRM. The objects were observed as backup targets for other programs, so the observing conditions were usually poor. The exposure time per object was between 3 and 10 min. We have observed roughly 40 objects to date. The near-IR images were reduced using standard IRAF[7] routines. The near-IR photometry is used to separate quasars from late-type dwarf stars, which are the primary contaminants in i-dropout searches, as mentioned earlier. Stars can be rejected based on the $z-J$ versus $i-z$ color-color diagram; a more detailed description can be found in Jiang et al. (2008, 2009). In short, we use the following criterion to further select quasar candidates,

$$z - J < 0.5(i - z) + 0.5. \quad (5)$$

In the final step we conducted optical spectroscopy to identify quasar candidates using the MMT Red Channel spectrograph. We have observed about 10 candidates, preferentially choosing candidates with UKIDSS photometry in the Y and J bands. The $Y-J$ color is one of the best criteria for separating $z \sim 6$ quasars L and T dwarfs. The MMT observations were made in long-slit mode with a spectral resolution of $\sim$10 Å. The exposure times for each target were 5–10 min, sufficient to classify our candidates as quasars under normal weather conditions. If a target was identified as a quasar immediately after its first spectrum was obtained, additional 5 or 10 min exposures were taken to improve the spectral quality. Two quasars were identified with poor observing conditions, and their additional spectra were taken one year later. The spectra of one quasar (SDSS J0842+1218) was obtained with Keck/ESI. The spectra were reduced using standard IRAF routines. In total we identified eight new quasars from the optical spectroscopic observations.

4. RESULTS AND DISCUSSION

4.1. *Discovery of Eight New Quasars at $z \sim 6$*

In this section we present the discovery of eight new quasars at $z \sim 6$. Table 2 lists the coordinates, redshifts, and optical and near-IR photometry of the new quasars. The naming convention for SDSS sources is SDSS JHHMMSS.SS±DDMMSS.S, and the positions

[7] IRAF is distributed by the National Optical Astronomy Observatory, which is operated by the Association of Universities for Research in Astronomy (AURA) under cooperative agreement with the National Science Foundation.

Table 2
Eight New Quasars in the SDSS Overlap Regions

Quasar (SDSS)	Redshift	i (mag)[a]	z (mag)[a]	MJD[b]	Y (mag)	J (mag)
J000825.77–062604.6	5.929±0.003	23.91±0.65	20.04±0.15	53997		19.43±0.13
		24.04±1.03	19.55±0.13	55120		
		22.85±0.25	20.35±0.09	56561		
J002806.57+045725.3	6.04±0.03	22.73±0.27	20.30±0.14	54742	19.59±0.09[c]	19.16±0.12[c]
		>24	20.42±0.22	54764		
		24.00±0.50	20.49±0.10	56560		
J014837.64+060020.0	5.923±0.003	22.25±0.18	19.31±0.06	53655	18.91±0.06[c]	18.37±0.07[c]
		22.09±0.22	19.35±0.08	53654		
J084229.43+121850.5	6.055±0.003	23.31±0.39	19.56±0.08	53441		18.84±0.03
		23.43±0.72	19.46±0.12	53684		
J085048.25+324647.9	5.867±0.007	24.25±0.78	20.34±0.16	52664		18.90±0.10
		23.66±0.52	20.39±0.15	52664		
			19.95±0.08	56369		
J120737.43+063010.1	6.040±0.003	22.70±0.29	20.16±0.12	52338	19.51±0.09[c]	19.35±0.14[c]
		23.49±0.61	20.17±0.16	52435		
		>23.5	20.39±0.11	56370		
J125757.47+634937.2	6.02±0.03	24.91±0.84	20.20±0.15	51987	20.39±0.16	19.78±0.08
		23.55±0.54	20.29±0.14	51633		
		23.50±0.40	20.60±0.12	56394		
J140319.13+090250.9	5.86±0.03	22.53±0.23	20.17±0.14	52757	19.70±0.12[c]	19.17±0.10[c]
		23.01±0.32	20.26±0.13	52345		
		22.73±0.22	20.48±0.11	56394		

[a] The first two entries for each quasar were from the SDSS, and the third entry (if there is one) was from the Bok 90Prime.
[b] MJD for the i and z-band photometry.
[c] Photometry from the UKIDSS.

are expressed in J2000.0 coordinates. We use SDSS JHHMM±DDMM (or JHHMM in figures) for brevity. The new quasars span a relatively narrow redshift range of $5.86 < z < 6.06$. The redshifts were mostly measured from several emission lines including Lyα, O I λ1304 (hereafter O I), C II λ1335 (hereafter C II), and Si IV λ1396 (hereafter Si IV), by fitting a Gaussian profile to the top $20 \sim 50\%$ of these lines. Three quasars do not show apparent line emission in their optical spectra, so their redshifts were measured from the wavelength where the sharp flux decline occurs. They are discussed in more detail in the next subsection. The redshift errors quoted in Table 2 include the uncertainties from our fitting process and wavelength calibration. They do not include any possible velocity shifts between these lines and systemic redshifts. For the quasars without apparent line emission, we adopted a redshift error of 0.03, corresponding to the scatter in the relation between Lyα redshifts and systemic redshifts (e.g. Shen et al. 2007). Two of the quasars (SDSS J0148+0600 and SDSS J1207+0630) were independently discovered by S. Warren et al. (in preparation).

In Table 2, there are multiple entries for the i and z band photometry. The first two entries for each quasar are the duplicate observations from the SDSS, and the third one (if present) is the improved photometry from Bok 90Prime. Figure 3 shows two examples of the multi-epoch observations of the quasars SDSS J0008–0626 and SDSS J0028+0457. In the SDSS observations (Epochs 1 and 2), the two quasars were not (or barely) detected in the i band, and were very weak ($5\sigma - 7\sigma$) in the z band. In the Bok 90Prime observations (Epoch 3) they are clearly detected in the i band, and have strong detections ($\geq 10\sigma$) in the z band. Note that quasars are variable objects with a typical variability amplitude of a few tenths of a magnitude (e.g. MacLeod et al. 2012), so the difference of the photometry in different entries for the same quasar may partially reflect this variability. SDSS J0148+0600 and SDSS J0842+1218 do not have the third entry of the i and z band photometry. They are more than 10σ detections in the SDSS observations, so we did not take more images for them. The other six quasars are weaker than 10σ detections, which was the limit in the previous survey of $z \sim 6$ quasars with the SDSS single-epoch images.

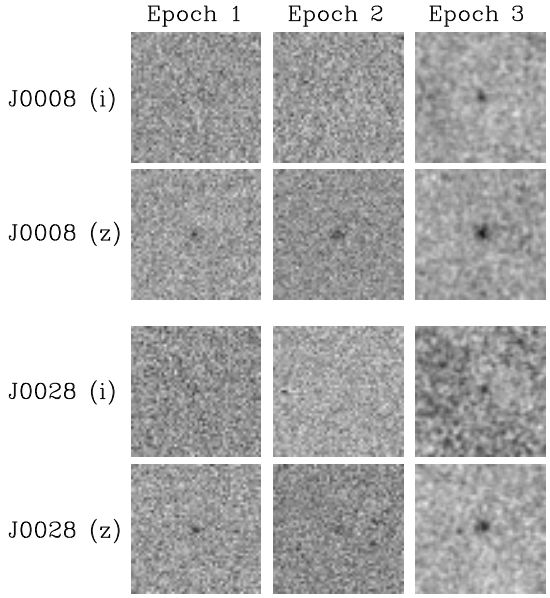

Figure 3. Multi-epoch observations of SDSS J0008–0626 and SDSS J0028+0457 in the i and z bands. In the SDSS observations (Epoch 1 and 2), the two quasars were not (or barely) detected in the i band, and were very weak ($5\sigma - 7\sigma$) in the z band. The new Bok 90Prime observations (Epoch 3) clearly detected them in the i band, and have strong detections ($\geq 10\sigma$) in the z band.

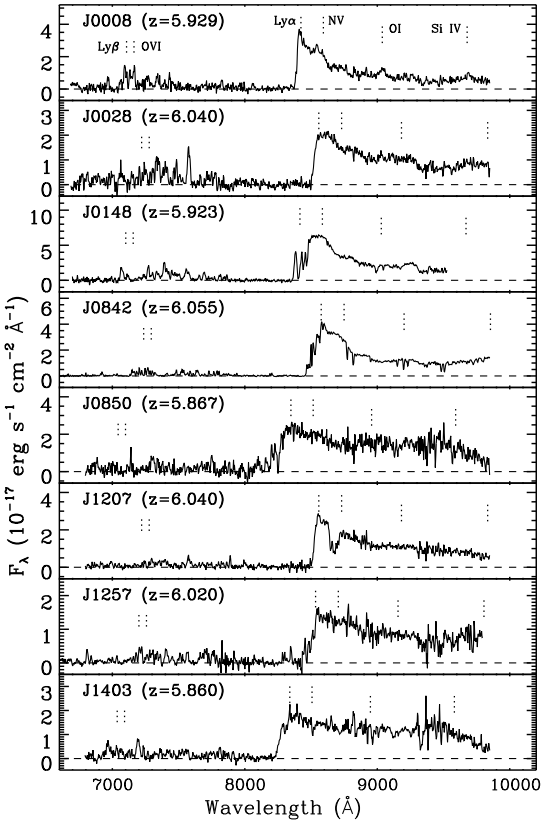

Figure 4. Optical spectra of the eight quasars. The spectrum of SDSS J0842+1218 was taken from Keck/ESI. The spectra of the other quasars were taken from the MMT Red Channel Spectrograph. Each spectrum has been scaled to match the corresponding z-band magnitude in Table 1, thereby placed on an absolute flux scale.

The last two columns of Table 2 show the near-IR (Y and J) photometry. The Y and J band photometry for four quasars was obtained from the UKIDSS. As we mentioned in section 3.3, in this first study we preferentially observed candidates with UKIDSS Y and J-band photometry. The near-IR photometry of the other four quasars was obtained with the MMT SWIRC.

Figure 4 shows the optical spectra of the quasars. As addressed in section 3.3, one quasar (SDSS J0842+1218) was observed with Keck/ESI, and its total integration time was 20 min. The other seven quasars were observed with the MMT Red Channel Spectrograph. The total integration time per object was from 10 min to 40 min, depending on the quasar brightness and observing conditions. Each spectrum in Figure 4 has been scaled to match the best corresponding z-band magnitude in Table 1, thereby placed on an absolute flux scale. These quasars show a diversity of Lyα emission. For example, SDSS J0008–0626 and SDSS J0842+1218 have strong Lyα emission lines. SDSS J0148+0600 and SDSS J1207+0630 are likely broad absorption line (BAL) quasars. SDSS J1257+6349 and SDSS J1403+0902 do not show any prominent Lyα emission. Quasars with weak emission lines like these quasars are not rare at high redshift. We have found a significant fraction of lineless quasars at $z \sim 6$ (e.g. Jiang et al. 2009; Bañados et al. 2014).

Table 3 shows the properties of the quasar continua and Lyα emission lines. Columns 3 and 4 list m_{1450} and M_{1450}, the apparent and absolute AB magnitudes of the continuum at rest-frame 1450 Å. They were calculated by fitting a power-law continuum $f_\nu \sim \nu^{\alpha_\nu}$ to the spectrum of each quasar. Our optical spectra only cover a short wavelength range in the rest frame ($100 \sim 150$ Å), and this range contains several UV emission lines, so we were not able to reliably measure the slopes of the continua. We assumed that the slope is the average quasar UV continuum slope $\alpha_\nu = -0.5$ (e.g. Vanden Berk et al. 2001). The power-law continuum was then normalized to match visually identified continuum windows with little contribution from line emission. After the power-law continuum was subtracted from the spectrum, we measured the rest-frame equivalent width (EW) of the Lyα emission line, including the N V λ1240 (hereafter N V) line that is usually blended with Lyα. This was done by fitting a half Gaussian profile (Lyα) and a full Gaussian profile (N V) simultaneously to the spectrum redward of the Lyα line center. We ignored the weak Si II λ1262 emission line on the red side of N V. For the quasars without prominent Lyα emission, we simply integrated flux (instead of Gaussian fitting) above the continuum. We did not correct for the flux absorbed by the Lyα forest. The results are shown in Column 5 in Table 3. These measurements are crude due to uncertainties from continuum measurement, redshift determination, and Lyα forest absorption.

4.2. *Notes on Individual Objects*

SDSS J0008–0626 (z=5.929). SDSS J0008–0626 has a strong Lyα emission line. It also shows prominent N V, O I, and Si IV emission lines. Its redshift was measured from the O I emission line.

SDSS J0028+0457 (z=6.04). SDSS J0028+0457 was independently discovered by the Pan-STARRS1 survey (Bañados et al. 2014). It does not have prominent emission lines in the spectrum shown in Figure 4. The redshift measured from the weak Lyα line peak is 6.09, and the redshift measured from the wavelength where the sharp flux drop occurs is 6.04. Here we adopt 6.04. This is slightly higher than the redshift reported in Bañados et al. (2014) (z =5.99). An interesting feature is a strong narrow emission line at $\lambda = 7580$ Å. It exists in all three individual MMT spectra, as well as the Bañados et al. (2014) spectrum, so it is a real line feature. It could be a luminous Lyα emitter at $z = 5.23$, or an ionized IGM bubble at $z = 5.23$. Higher resolution imaging and spectroscopy are needed to explore the nature of this line.

SDSS J0148+0600 (z=5.923). SDSS J0148+0600 is the brightest quasar in this sample. It was well detected in the SDSS single-epoch images and the UKIDSS near-IR images. It is likely a low-ionization BAL (LoBAL) quasar, and its Lyα emission line has been mostly absorbed. The EW listed in Table 3 is a lower limit. It does not have obvious emission lines other than C II redward of N V in its optical spectrum, so we used C II to determine the redshift. This quasar was independently discovered by S. Warren et al. (in preparation). Becker et al. (2015) found that it showed a very long Gunn-Peterson trough in a deep VLT/X-Shooter spectrum.

SDSS J0842+1218 (z=6.055). SDSS J0842+1218 was

Table 3
Properties of Continua and Emission Lines

Quasar (SDSS)	Redshift	m_{1450} (mag)	M_{1450} (mag)	$\mathrm{EW_{Ly\alpha+NV}}$ (Å)
J0008–0626	5.929	20.63±0.09	–26.04±0.09	78
J0028+0457	6.040	20.34±0.10	–26.38±0.10	17
J0148+0600	5.923	19.60±0.06	–27.08±0.06	> 87
J0842+1218	6.055	19.85±0.09	–26.85±0.09	44
J0850+3246	5.867	19.92±0.08	–26.74±0.08	10
J1207+0630	6.040	20.10±0.11	–26.60±0.11	31
J1257+6349	6.02	20.56±0.12	–26.14±0.12	18
J1403+0902	5.86	20.39±0.11	–26.27±0.11	8

discovered in 2007. Its optical spectrum was obtained with Keck/ESI (20 min exposure in total). It has been observed in the near-IR and mid-IR wavelength ranges, and its physical properties such as metallicity and black hole mass have been well measured (e.g. Jiang et al. 2010; De Rosa et al. 2011). This quasar was initially selected from the SDSS single-epoch images, but also satisfies our overlap region selection criteria. We include this quasar because it is in the overlap regions and its optical spectrum was never published. The redshift of this quasar measured from the Lyα line is 6.055. This is consistent with the redshift 6.08 measured from its Mg II emission line (De Rosa et al. 2011), given the large scatter (~ 0.03) between Lyα redshifts and systemic redshifts.

SDSS J0850+3246 (z=5.867). SDSS J0850+3246 shows a very weak Lyα emission line with an observed rest-frame EW about 10Å. It does not show any other line emission in its optical spectrum in Figure 4.

SDSS J1207+0630 (z=6.040). SDSS J1207+0630 is a high-ionization BAL (HiBAL) quasar, as seen from the strong N V absorption line in the spectrum. It was also covered and detected in the near-IR by the UKIDSS.

SDSS J1257+6349 (z=6.02). SDSS J1257+6349 does not show any significant line emission in its optical spectrum in Figure 4. Its redshift was measured from the sharp flux drop at the Lyα line.

SDSS J1403+0902 (z=5.860). SDSS J1403+0902 is another weak line quasar, with an observed rest-frame Lyα EW of only 8Å. Its redshift was measured from the sharp flux drop at the Lyα line. It was also covered and detected in the near-IR by the UKIDSS.

4.3. *Discussion*

The currently known SDSS quasars at $z \sim 6$ were selected either from single-epoch imaging data encompassing more than 8000 deg^2 with a limiting depth of $z_{\rm AB} \sim 20$ mag, or from the Stripe 82 multi-epoch co-added images over 300 deg^2 that are two magnitudes deeper. The SDSS overlap regions provide another unique dataset that is in between the SDSS single-epoch data and the Stripe 82 data in terms of areal coverage and image d epth. These regions cover roughly 3700 deg^2 area at $|b| > 30°$, which is nearly one third of the total SDSS sky coverage, and is an order of magnitude greater than the area of Stripe 82. We have demonstrated that the overlap regions can be used to efficiently select quasar candidates that are $\gtrsim$0.5 mag fainter than those found in single-epoch images. Duplicate observations allow us to select fainter $z \sim 6$ candidates primarily because the initial candidate selection is largely free of spurious detections. The survey limit for $z \sim 6$ quasars in single-epoch images was roughly $z_{\rm AB} = 20$ mag (or 10σ detections). Beyond this limit, the number of spurious detections increases dramatically, making follow-up observations infeasible. The multi-epoch observations in the overlap regions ensure that the majority of single-band (z-band) detections are real.

In our first quasar search we have found eight quasars in the overlap regions. We also recovered several known quasars that are located in the overlap regions. As we mentioned earlier, the follow-up observations of our candidates have not been systematic. They were usually observed as backup targets in other programs, when weather conditions were poor. Hence these quasars do not form a statistically complete sample. However, they provide guidance for a future systematic quasar survey over the whole overlap regions. In addition, we will use the WISE mid-IR imaging data to improve our selection efficiency (e.g. Wu et al. 2012; Carnall et al. 2015).

5. SUMMARY

In this paper we have presented the discovery of eight new quasars at $z \sim 6$. They were found in our first high-redshift quasar search in the SDSS overlap regions. These regions were scanned twice or more by the SDSS imaging survey, allowing us to select quasars fainter than those found in SDSS single-epoch images. We have introduced the details of our quasar selection procedure, including the selection of i-band dropouts, the follow-up optical and near-IR imaging observations, and the final spectroscopic identifications. The eight quasars span a redshift range of $5.86 < z < 6.06$. Five of them are fainter than $z_{\rm AB} = 20$ mag, and the faintest one is $z_{\rm AB} = 20.6$ mag, $\sim$0.5 mag fainter than those found from SDSS single-epoch images. These quasars show a diversity of emission line properties in their optical spectra, from strong emission lines to lineless features. In addition, we recovered eight previously known $z \sim 6$ quasars that are also located in these overlap regions. These results indicate that the SDSS overlap regions can be used to efficiently select high-redshift quasars. We plan to carry out a systematic survey of $z \sim 6$ quasars in the whole SDSS overlap regions at high galactic latitude.

We acknowledge the support from a 985 project at Peking University. L.J. and Z.F. acknowledge supports from the National Natural Science Foundation of China (NSFC) under grants 11003021 and 11373003. X.F. and I.D.M. acknowledge support from U.S. NSF grant AST

11-07682. Observations reported here were obtained in part at the MMT Observatory, a joint facility of the University of Arizona and the Smithsonian Institution. This work is based in part on observations at KPNO, NOAO (Prop. ID: 2014B-0099; PI: Linhua Jiang), which is operated by the AURA under cooperative agreement with the NSF. This work is based in part on data obtained as part of the UKIRT Infrared Deep Sky Survey. This research has benefited from the M, L, T, and Y dwarf compendium housed at DwarfArchives.org.

Funding for the SDSS and SDSS-II has been provided by the Alfred P. Sloan Foundation, the Participating Institutions, the National Science Foundation, the U.S. Department of Energy, the National Aeronautics and Space Administration, the Japanese Monbukagakusho, the Max Planck Society, and the Higher Education Funding Council for England. The SDSS Web Site is http://www.sdss.org/. The SDSS is managed by the Astrophysical Research Consortium for the Participating Institutions. The participating institutions are the American Museum of Natural History, Astrophysical Institute Potsdam, University of Basel, University of Cambridge, Case Western Reserve University, University of Chicago, Drexel University, Fermilab, the Institute for Advanced Study, the Japan Participation Group, Johns Hopkins University, the Joint Institute for Nuclear Astrophysics, the Kavli Institute for Particle Astrophysics and Cosmology, the Korean Scientist Group, the Chinese Academy of Sciences (LAMOST), Los Alamos National Laboratory, the Max-Planck-Institute for Astronomy (MPIA), the Max-Planck-Institute for Astrophysics (MPA), New Mexico State University, Ohio State University, University of Pittsburgh, University of Portsmouth, Princeton University, the United States Naval Observatory, and the University of Washington.

Facilities: Bok (90Prime), MMT (SWIRC, Red Channel spectrograph), Mayall (NEWFIRM), Keck (ESI)

REFERENCES

Annis, J., Soares-Santos, M., Strauss, M. A., et al. 2014, ApJ, 794, 120
Bañados, E., Venemans, B. P., Morganson, E., et al. 2014, AJ, 148, 14
Becker, R. H., Fan, X., White, R. L., et al. 2001, AJ, 122, 2850
Becker, G. D., Bolton, J. S., Madau, P., et al. 2015, MNRAS, 447, 3402
Bertin, E., & Arnouts, S. 1996, A&AS, 117, 393
Bertin, E. 2006, in ASP Conf. Ser. 351, Astronomical Data Analysis Software and Systems XV, ed. C. Gabriel, C. Arviset, D. Ponz, & E. Solano (San Francisco, CA: ASP), 112
Brown, W. R., McLeod, B. A., Geary, J. C., & Bowsher, E. C. 2008, Proc. SPIE, 7014, 90
Carilli, C. L., Wang, R., Fan, X., et al. 2010, ApJ, 714, 834
Carnall, A. C., Shanks, T., Chehade, B., et al. 2015, arXiv:1502.07748
De Rosa, G., Decarli, R., Walter, F., et al. 2011, ApJ, 739, 56
Fan, X., White, R. L., Davis, M., et al. 2000, AJ, 120, 1167
Fan, X., Narayanan, V. K., Lupton, R. H., et al. 2001, AJ, 122, 2833
Fan, X., Strauss, M. A., Schneider, D. P., et al. 2003, AJ, 125, 1649
Fan, X., Hennawi, J. F., Richards, G. T., et al. 2004, AJ, 128, 515
Fan, X., Strauss, M. A., Richards, G. T., et al. 2006, AJ, 131, 1203
Fan, X., Strauss, M. A., Becker, R. H., et al. 2006, AJ, 132, 117
Fukugita, M., Ichikawa, T., Gunn, J. E., et al. 1996, AJ, 111, 1748
Goto, T. 2006, MNRAS, 371, 769
Gunn, J. E., Carr, M., Rockosi, C., et al. 1998, AJ, 116, 3040
Gunn, J. E., Siegmund, W. A., Mannery, E. J., et al. 2006, AJ, 131, 2332
Hogg, D. W., Finkbeiner, D. P., Schlegel, D. J., & Gunn, J. E. 2001, AJ, 122, 2129
Ivezić, Ž., Lupton, R. H., Schlegel, D., et al. 2004, Astronomische Nachrichten, 325, 583
Jiang, L., Fan, X., Vestergaard, M., et al. 2007, AJ, 134, 1150
Jiang, L., Fan, X., Annis, J., et al. 2008, AJ, 135, 1057
Jiang, L., Fan, X., Bian, F., et al. 2009, AJ, 138, 305
Jiang, L., Fan, X., Brandt, W. N., et al. 2010, Nature, 464, 380
Jiang, L., Fan, X., Bian, F., et al. 2014, ApJS, 213, 12
Kurk, J. D., Walter, F., Fan, X., et al. 2007, ApJ, 669, 32
Lawrence, A., Warren, S. J., Almaini, O., et al. 2007, MNRAS, 379, 1599
Lupton, R. H., Gunn, J. E., & Szalay, A. S. 1999, AJ, 118, 1406
MacLeod, C. L., Ivezić, Ž., Sesar, B., et al. 2012, ApJ, 753, 106
McGreer, I. D., Mesinger, A., & Fan, X. 2011, MNRAS, 415, 3237
Morganson, E., De Rosa, G., Decarli, R., et al. 2012, AJ, 143, 142
Mortlock, D. J., Patel, M., Warren, S. J., et al. 2009, A&A, 505, 97
Mortlock, D. J., Warren, S. J., Venemans, B. P., et al. 2011, Nature, 474, 616
Shen, Y., Strauss, M. A., Oguri, M., et al. 2007, AJ, 133, 2222
Skrutskie, M. F., Cutri, R. M., Stiening, R., et al. 2006, AJ, 131, 1163
Stoughton, C., Lupton, R. H., Bernardi, M., et al. 2002, AJ, 123, 485
Vanden Berk, D. E., et al. 2001, AJ, 122, 549
Venemans, B. P., McMahon, R. G., Warren, S. J., et al. 2007, MNRAS, 376, L76
Venemans, B. P., Findlay, J. R., Sutherland, W. J., et al. 2013, ApJ, 779, 24
Venemans, B. P., Bañados, E., Decarli, R., et al. 2015, ApJ, 801, 11
Walter, F., Riechers, D., Cox, P., et al. 2009, Nature, 457, 699
Wang, R., Wagg, J., Carilli, C. L., et al. 2011, AJ, 142, 101
Wang, R., Wagg, J., Carilli, C. L., et al. 2013, ApJ, 773, 44
Warren, S. J., Hambly, N. C., Dye, S., et al. 2007, MNRAS, 375, 213
Willott, C. J., Delfosse, X., Forveille, T., Delorme, P., & Gwyn, S. D. J. 2005, ApJ, 633, 630
Willott, C. J., Delorme, P., Omont, A., et al. 2007, AJ, 134, 2435
Willott, C. J., Delorme, P., Reylé, C., et al. 2009, AJ, 137, 3541
Willott, C. J., Delorme, P., Reylé, C., et al. 2010, AJ, 139, 906
Wu, X.-B., Hao, G., Jia, Z., Zhang, Y., & Peng, N. 2012, AJ, 144, 49
York, D. G., Adelman, J., Anderson, J. E., Jr., et al. 2000, AJ, 120, 1579